Microphysical modes of precipitation growth determined by vertically pointing radar at Locarno-Monti during MAP

Sandra E. Yuter and Robert A. Houze, Jr.,
Department of Atmospheric Sciences, University of Washington, Seattle, WA 98195

1. Introduction

Heavy rain of the type that produces flooding in the Alps must be produced both quickly and efficiently over the lower slopes of the alpine barrier. Cloud water condensed over the terrain must be swept out rapidly by precipitation particles. Riming (collection of cloud water by ice particles) above the 0°C level and coalescence (collection of cloud water by raindrops) below the freezing level may both contribute to this process. An assessment of the relative contributions of these processes to the accretional growth of precipitation is important in estimating precipitation efficiency (Smith 1979).

This paper presents preliminary results regarding an assessment of the relative roles of riming and coalescence in the same column of precipitating cloud using vertically pointing radar data obtained during the Mesoscale Alpine Programme (MAP, Houze et al. 1998; Bougeault et al. 2001). The University of Washington Orographic Precipitation Radar (OPRA) is a vertically pointing 10-cm meteorological pulsed Doppler radar (Table 1). OPRA was deployed from September-October 1999 at Locarno-Monti in collaboration with Jürg Joss and Urs Germann of the Swiss Meteorological Agency. Approximately 365 hours of radar data were obtained during 11 of the MAP Intensive Observation Periods (IOPs).

Previous studies have assigned a dominant precipitation growth process to particular time periods of vertically pointing radar data. W est et al. (2000) classified degree of riming (Moismann et al. 1994) over 30-min periods using Formvar data of ice particles obtained concurrently with vertically pointing radar data. White et al. (2001) classified the precipitation growth mechanism in 30-min blocks of vertically pointing radar data using the mean vertical profile of reflectivity and the presence or absence of a radar bright band. We approach the problem from a different perspective by addressing the relative contributions of riming and coalescence within the *same* column of 1-sec data. The vertical profile of the vertical velocity of air (w) is critical to understanding the relationship between coalescence and riming. We first estimate characteristics of the vertical profile of w using the observed Doppler velocity (V_r) data and reflectivity-weighted fall speeds ($<V_t>$) derived from observed reflectivity (Z). From a profile of estimated w with height, we then use Kessler s 1-D water continuity model (Kessler 1967) to assess the relative rates of collection of cloud water in regions above and below 0°C.

2. Data

The OPRA data consists of vertical profiles of radar reflectivity, Doppler velocity, and spectral width obtained every 1 sec at 150-m vertical resolution to a height of ~7 km AGL. The horizontal resolution of the data varies with the advection speed of the precipitating elements over the radar. For typical advection speeds of 3 to 10 m s^{-1}, the resulting horizontal resolution of the data is 3 to 10 meters for a 1 sec profile. Figure 1 shows 45 min of OPRA data obtained during MAP IOP2b on 20 September 1999. From 0700-0725 UTC a region of heavy precipitation is indicated by the strong reflectivity values in rain and snow. The 0°C level is at ~3-km altitude. Fallstreaks are evident both above 0°C level within snow and below within rain. A ~300-m wide layer of enhanced reflectivities is associated with melting particles in the heavy precipitation. After 0725 UTC, the convection weakens and lighter precipitation falls for ~15 min followed by moderate precipitation from 0740-0750 UTC. During the weaker precipitation, the layer of enhanced reflectivities associated with the melting of snow is narrower and slightly weaker than during the heavier precipitation. Although the absolute magnitudes of the reflectivity in the light precipitation melting layer are smaller, their relative magnitudes compared to the rain region below are larger, and hence the melting band is more distinct. The ultra high resolution OPRA data reveal nearly ubiquitous small-scale fallstreaks in a wide range of intensities of precipitation from light to heavy. Fallstreaks in rain appear to originate in locally intense regions within the melting layer and may connect to a fallstreak in snow descending from above.

3. Estimation of characteristics of vertical velocity profile

a. Derivation of vertical air velocity in rain

The observed mean Doppler velocity represents the sum of the average air velocity and the mean reflectivity-weighted fall speed of the raindrops in the resolution volume ($V_r = w + <V_t>$). If one knew the actual distribution of raindrops within the radar resolution volume, and the temperature and pressure, one could apply an empirical diameter to fall speed relation (e.g. Gunn and Kinzer 1949) to derive the distribution of fall speeds for the raindrop size distribution (DSD) and from that compute the mean reflectivity-weighted fall speed for the DSD.

A basic practical problem with deriving w from V_r data is that the actual DSD in the radar resolution volume is unknown. Methods are available to estimate some characteristics of the DSD from a recording of the full Doppler spectra (e.g. Gossard et al. 1990). However, OPRA was able to measure only the mean Doppler velocity values as larger integration times are required to record a reliable full Doppler spectrum for each range gate.

Joss (personal communication, 2000) has shown that use of a wide range of assumptions regarding the form of a gamma distribution DSD from nearly monodisperse (m = 16) to exponential (m = 0) yields estimates of reflectivity-weighted average fall speed within ~1.5 m s^{-1}. This worse case uncertainty of ~1.5 m s^{-1} is comparable to the uncertainty of aircraft in situ w measurements.

Sets of Z and $\langle V_t \rangle$ values were calculated for different sets of assumptions regarding rain rate, m, N_o of the DSDs and variations in temperature and pressure. These data were then fit to an equation of the form $\langle V_t \rangle = b + kZ$ in order to analytically determine the coefficients b and k as a function of m, N_o, temperature, and pressure. Turbulence is assumed to be symmetric such that over the radar resolution volume its mean is zero.

As a test of the feasibility of the method, it was applied to several samples of OPRA data. The lapse rate was assumed to be 6 deg km^{-1} and the pressure decreased by a factor of exp(height/10) where height is in km. The calculations were made assuming the DSD was exponential (i.e., $m = 0$), which is consistent with DSD observations at larger sample sizes approaching the scale of a radar volume (e.g. Joss and Gori 1978) and assigning $N_o = 8000$ (Marshall and Palmer 1948). Vertical velocity was estimated at each range gate in each radar data profile independently (i.e., no mass continuity constraint was applied). The derived w results are shown in Figure 2 in terms of a contoured frequency by altitude diagram (CFAD) (Yuter and Houze 1995), a joint frequency distribution of w with height. Since Joss's method applies only to raindrops, the CFAD is truncated at 3-km altitude near the 0ºC level. An abrupt shift in the modal values of w occurs at 2.8-km altitude near the bottom of the melting layer. The CFAD shows that the strongest mode of the frequency distribution of w is near 0 m s^{-1} at all heights within rain (< 2.7-km altitude). This result is consistent with the frequency distribution of w based on studies of dual-Doppler data (e.g. Yuter and Houze 1995; Braun et al. 1997). Updrafts < 3 m s^{-1} predominate at low levels. The outliers of the distribution varied between approximately + 5 m s^{-1} for updrafts and – 6 m s^{-1} for downdrafts. Time-height plots of the estimated vertical velocity (not shown) indicate coherent updraft and downdraft structures. The results of these simple tests are promising in that Joss's method produced physically realistic results. An alternate version of the fall speed and derived w fields were also obtained from the OPRA data using the Atlas et al. (1973) mapping of reflectivity to fall speed of $V_t = 2.6Z^{0.107}$. When applied to the OPRA data, w values derived using the Atlas et al. (1973) formula yielded a distribution of w values with a physically inconsistent negative bias.

b. Derivation of vertical air velocity in snow

Ice crystals of different habits have different mass-to-size relationships and hence different fall speed relations for the same diameter, temperature, and pressure. Locatelli and Hobbs (1974) measured the fall velocities of a variety of snow particles of different crystal habits. Hanesch (1999) obtained snow particle to fall speed relations for several degrees of riming using 2-D video disdrometer data obtained during the Swiss Alpine Melting Layer Measurements campaign in winter 1996/1997. Both analyses found that most naturally occurring snow particles had fall speeds in still air from near 0 to 2 m s^{-1} and small graupel (5 mm diameter) had fall speeds of ~3 m s^{-1}.

In order to estimate the fall speed of ice from reflectivity, a crystal habit and associated fall speed relation with size would need to be assumed. As a first step, a simple method that does not require information about the particle size distribution is used to estimate a lower bound for the vertical air motions in snow. The observed Doppler velocity data in snow are split into two groups. For $V_r > 0$ m s^{-1}, the observed Doppler velocity represents a robust underestimate of positive vertical air velocity. For $V_r \leq 0$ m s^{-1}, the physical interpretation is ambiguous. Using this simple method, one can examine the statistics of the underestimated positive vertical air velocities and interpret these velocities as characteristics of the vertical profile of w. When this method is applied to samples of OPRA data, maximum V_r of ~ 2 m s^{-1} are observed near the 3.5-km altitude.

Preliminary analysis of subsets of OPRA data using the two methods described above yields vertical velocities between 2 and 5 m s^{-1} as defensible estimates of the likely maximum vertical velocities within updrafts associated with precipitation in Locarno-Monti during IOP2b. These velocities are assumed to occur as the local maximum within parabolic profiles of vertical velocity which are in turn are used as input to a 1-D microphysical parameterization described below.

4. Relative roles of different processes in precipitation growth

An estimation of the relative roles of several precipitation processes in the growth of precipitation was made using a simple 1-D column model calculation for a precipitating cold cloud following Kessler (1967), Ogura and Takahashi (1971), Ferrier (1988), and Houze (1993, Section 3.6). The following equations describe water continuity in terms of the rate of change of the mixing ratios of water vapor (q_v), cloud water (q_c), rain (q_r), and ice (q_i) in the simple model:

$$\frac{Dq_v}{Dt} = -C_c \qquad \frac{Dq_r}{Dt} = A_c + K_c - F_r - G_l$$

$$\frac{Dq_c}{Dt} = C_c - A_c - K_c - K_{ci} \qquad \frac{Dq_i}{Dt} = G_l + K_{ci} - F_i$$

where C_c is condensation of cloud water, A_c is autoconversion (the rate at which cloud water content decreases due to growth of precipitation by coalescence of cloud drops), K_c is the collection of cloud water by raindrops, K_{ci} is the collection of cloud water by graupel above the 0°C level, G_l is the glaciation of rain into ice, F_r is the fallout of raindrops from the air parcel, and F_i is the fallout of ice particles.

The parcel is assumed to be saturated with respect to liquid water at all temperatures (i.e., entrainment and evaporation are ignored). Integration starts at cloud base (z= 1 km) where $q_c = q_v = q_i = 0$ and $q_v = q_s$. The lapse rate was 6 K km^{-1} and temperature at 1000 hPa is 291 K based on Milan soundings for 20 September 1999. The fall speed of rain was set to 6 m s^{-1} and the fall speed for ice was set to a value for graupel of 3 m s^{-1}. Once the parcel is above the freezing level, the glaciation is assumed to be rapid such that by ~1 km above the freezing level all the preexisting rain has glaciated. Rapid glaciation is consistent with data obtained in several field studies (e.g. Yuter and Houze 1995; Zeng et al. 2001). The calculation is particularly sensitive to the assumptions regarding the glaciation rate and the fall speed relation of ice particles.

Several runs of the 1-D calculations were made using a parabolic profile of vertical air velocity from 1 to 7 km altitude and from 1 to 5 km altitude and assuming a 0ºC level at 3-km altitude. Figures 3 and 4 shows the calculations for maximum w of 2 m s^{-1} for a velocity profile extending to 7 km altitude and for maximum w of 5 m s^{-1} within a velocity

profile extending to 5-km altitude. The simplicity of the calculation limits our ability to make quantitative interpretations but some qualitative interpretations can be made. At weak-to-moderate vertical velocities observed in MAP IOP2b precipitation, the 2-km thick layer above the freezing level contains local maxima in q_i and K_{ci} indicating that this region is a favorable growth environment for graupel. Houze and Medina (2001) found graupel at these altitudes in dual-polarization radar data obtained by NCAR's SPOL radar in several MAP storms including IOP2b. A comparison of the relative rates of K_c below the freezing level and K_{ci} above the freezing level indicates that both collection of cloud water by rain and ice are important to the growth of precipitation and that neither can be ignored.

5. Conclusions

Preliminary analysis of the ultra high resolution (1 sec) vertically pointing S-band Doppler radar data obtained by the University of Washington OPRA indicates that fallstreaks are nearly ubiquitous in a wide range of precipitation intensities. At coarser resolution, convective cells are usually associated with radially symmetric vertically oriented reflectivity maxima. The OPRA data reveal that these cells are composed of small time and spatial scale variations in reflectivity that have expression as fallstreaks both above and below the 0ºC level. A subset of the fallstreaks has sufficient expression in reflectivity to indicate a clear connection across the melting layer from the snow to the rain region.

An estimation of characteristics of the vertical air velocity profile within precipitating cloud was made in both rain and snow regions using the observed radar parameters. In rain regions, reflectivity-weighted fall speed derived from the observed reflectivity using assumptions about the DSD and an empirical fall speed to diameter relation was subtracted from the observed Doppler velocity to yield an estimated *w*. In snow regions, a lower bound on maximum updraft *w* was estimated from the observed maximum Doppler velocity. Using these methods on data from MAP IOP2b, maximum vertical velocities in rain were ~5 m s^{-1} and minimum peak updraft velocities in snow were ~2 m s^{-1}.

Plausible parabolic vertical velocity profiles with maximum velocities between 2 to 5 m s^{-1} input into a simple calculation based on Kessler's 1-D water continuity equations yield local maxima in q_i (mixing ratio of ice) and K_{ci} (collection of cloud water by ice) within 2 km of the freezing level. These conditions constitute a favorable environment for graupel formation. Additionally, the model indicates that both coalescence and riming make significant contributions to the accretional growth of precipitation in these storms.

Future work will refine our methodologies and examine a larger data sample. We plan to improve the 1-D Kessler model to serve better as a tool to aid in the physical interpretation of the vertically pointing radar observations. In particular, we need to elaborate the characterization of precipitation growth and fallout. We will examine the sensitivity of the results to a wider range of assumptions regarding the *w* profile, and to the fall speed relations for a variety of graupel and snow types. We will also examine the tradeoffs regarding use of an idealized *w* profile for a parcel, as used here, versus the ensemble properties of the derived *w* field within the storm.

References

Atlas, D., R. C. Srivastava, and R. S. Sekhon, 1973: Doppler-radar characteristics of precipitation at vertical incidence. *Rev. Geophys. Space Phys*., **11**, 1-35.

Bougeault, P., and Coauthors, 2001: The MAP Special Observing Period. *Bull. Amer. Meteor. Soc.*, **82**, 433-462.

Braun, S. A., R. A. Houze, Jr., and B. F. Smull, 1997: Airborne dual-Doppler observations of an intense frontal system approaching the Pacific Northwest coast. *Mon. Wea. Rev*., **125**, 3131-3156.

Ferrier, B. S., 1988: One-dimensional time-dependent modeling of squall-line convection. Thesis (Ph.D.) #35283, University of Washington, Department of Atmospheric Sciences, 259 pp.

Gossard, E. E., R. G. Strauch, R. R. Rogers, 1990: Evolution of dropsize distributions in liquid precipitation observed by ground-based Doppler radar. *J. Atmos. Ocean. Tech.*, **7**, 815-828.

Gunn, R., and G. D. Kinzer, 1949: The terminal velocity of fall for water droplets in stagnant air. *J. Meteor.*, **6**, 243-248.

Hanesch, M., 1999: Fall velocity and shape of snowflakes. Ph.D. dissertation, ETH, Zurich, No. 13322, 117 pages.

Houze, R. A., Jr., 1993: *Cloud Dynamics*. Academic Press, San Diego, 573 pp.

Houze, R. A., Jr., J. Kuettner, and R. B. Smith, 1998: Mesoscale Alpine Programme. U. S. overview document and experimental design. 101 pp. [Available from MAP U.S. Project Office.]

Houze, R. A., Jr., and S. Medina, 2001: Alpine precipitation mechanisms in MAP IOP2b and IOP8. *Map Conf.*, Schliersee, Germany.

Joss, J., and E. G. Gori, 1978: Shapes of raindrop size distributions. *J. Appl. Meteor.*, **7**, 1054-1061.

Kessler, E., 1967: On the continuity of water substance. *ESSA Technical Memorandum* IERTM-NSSL 33, National Severe Storms Laboratory, Norman, OK, 125 pp.

Locatelli, J. D., and P. V. Hobbs, 1974: Fall speeds and masses of solid precipitation particles. *J. Geophys. Res*., **79**, 2185-2197.

Marshall, J. S., and W. McK. Palmer, 1948: The distribution of raindrops with size. *J. Meteor.*, **5**, 165-166.

Moismann, L., E. Weingartner, and A. Waldvogel, 1994: An analysis of accreted drop sizes and mass on rimed snow crystals. *J. Atmos. Sci*., **51**, 1548-1558.

Ogura, Y., and T. Takahashi, 1971: Numerical simulation of the life cycle of a thunderstorm cell. *Mon. Wea. Rev.*, **99**, 895-911.

Smith, R. B., 1979: The influence of mountains on the atmosphere. *Advances in Geophysics*, **21**, 87-230.

White, A. B., F. M. Ralph, P. J. Neiman, D. A. Kingsmill, and P. O. G. Persson, 2001: Process partitioning of rainfall enhanced by coastal orography. *Abstracts from Pacific Northwest Weather Workshop*, March 2-3 2001, Seattle, WA.

Wüest, M., W. Schmid, and J. Joss, 2000: Coupling between riming and the dynamics of precipitating clouds. *Proceedings 13th Internationational Conf. Clouds and Precipitation*, Reno, NV, 421-424.

Yuter S. E., and R. A. Houze, Jr., 1995: Three-dimensional kinematic and microphysical evolution of Florida cumulonimbus. Part II: Frequency distributions of vertical velocity, reflectivity, and differential reflectivity. *Mon. Wea. Rev.*, **123**, 1941-1963.

Zeng, Z., S. E. Yuter, R. A. Houze, Jr., and D. E. Kingsmill, 2001: Microphysics of the rapid development of heavy convective precipitation. *Mon. Wea. Rev.*, in press.

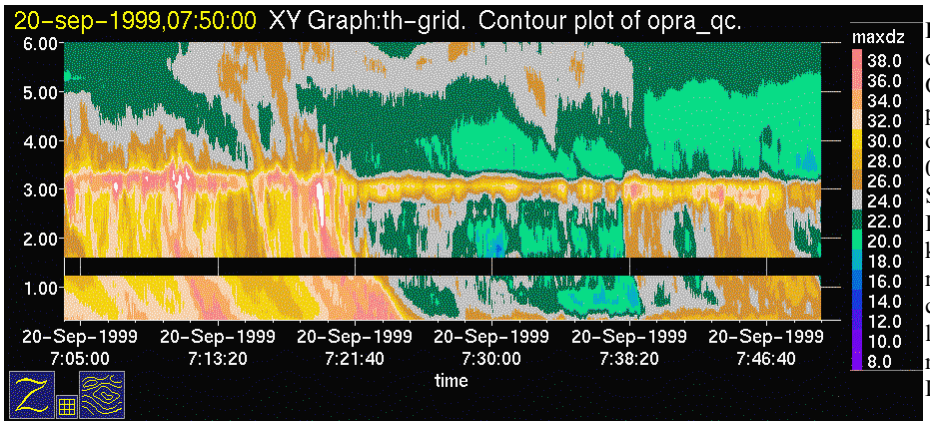

Figure 1. Contour plot of 45 min of 1 sec OPRA reflectivity profiles (2700 profiles) obtained from 0705-0750 UTC on 20 September 1999 during IOP2b. The data at 1.5 km altitude were removed as they were contaminated by side lobe echo from the mountains across the Lago-Maggiore valley.

Table 1. Characteristics of University of Washington Orographic Precipitation Radar (OPRA) during MAP.

Model	Modified Raytheon Pathfinder S-band
Receiver	NCAR/ATI PIRAQ
Signal Processor	50 MHz TI TMS320C50 on PIRAQ board
Host Computer	233 MHz Pentium II MMX, 32 MB RAM, 4 GB disk, DAT, CDROM
Frequency	3050 MHz
Antenna	1.8 m offset-feed parabola
Antenna Gain	31 dB (estimated)
Transmitter	Magnetron, 2J75B with solid state modulator
Peak Power	60 KW maximum, 35 KW minimum
Beam Width	4.3 deg (estimated)
PRF	1000 Hz
Pulse Width	1.0 microsec
# Gates	100
Variables	*Z*, *Vr*, and *SW*

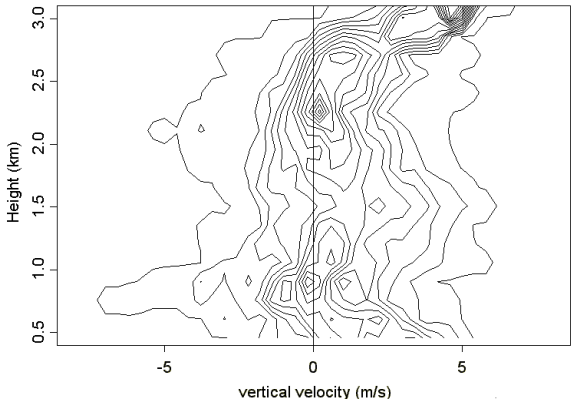

Figure 2. Joint probability distribution of the vertical air velocity versus height calculated for w bin size of 0.2 m s^{-1} & height bin size of 150 m for data obtained from 0704-0750 UTC 20 September 1999.

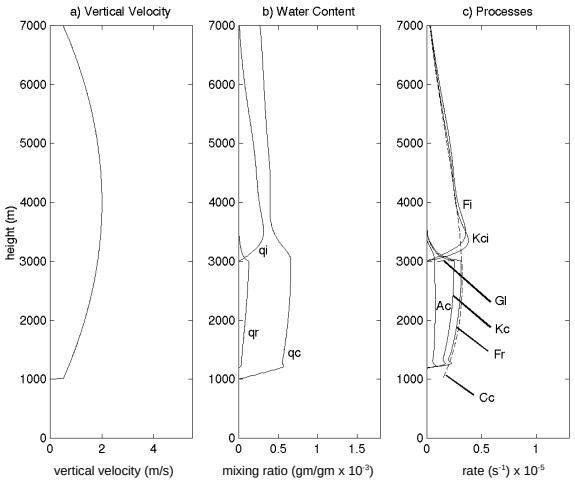

Figure 3. (a) Vertical velocity profile with max w= 2 m s^{-1} and updraft top of 7 km used as input to Kessler 1D model. Vertical profiles of model output in terms of (b) mixing ratios and (c) precipitation process rates. See text for explanation of symbols and further details.

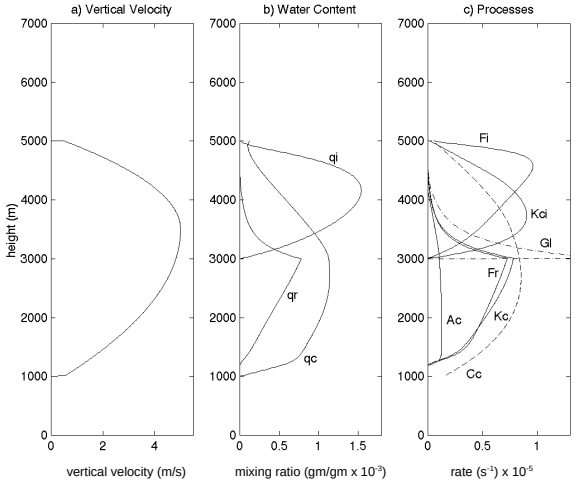

Figure 4. Similar to Figure 3 except vertical velocity profile in (a) with max w = 5 m s^{-1} and updraft top of 5 km used as input.